Appl. Phys. B (2017) 123:29
DOI 10.1007/s00340-016-6622-6

Applied Physics B
Lasers and Optics

Continuous-wave mid-infrared photonic crystal light emitters at room temperature

Binbin Weng[1] · Jijun Qiu[1,2] · Zhisheng Shi[1,2]

Received: 14 September 2016 / Accepted: 19 December 2016

Abstract Mid-infrared photonic crystal enhanced lead-salt light emitters operating under continuous-wave mode at room temperature were investigated in this work. For the device, an active region consisting of 9 pairs of PbSe/$Pb_{0.96}Sr_{0.04}Se$ quantum wells was grown by molecular beam epitaxy method on top of a Si(111) substrate which was initially dry-etched with a two-dimensional photonic crystal structure in a pattern of hexagonal holes. Because of the photonic crystal structure, an optical band gap between 3.49 and 3.58 μm was formed, which matched with the light emission spectrum of the quantum wells at room temperature. As a result, under optical pumping, using a near-infrared continuous-wave semiconductor laser, the device exhibited strong photonic crystal band-edge mode emissions and delivered over 26.5 times higher emission efficiency compared to the one without photonic crystal structure. The output power obtained was up to 7.68 mW (the corresponding power density was ~363 mW/cm^2), and a maximum quantum efficiency reached to 1.2%. Such photonic crystal emitters can be used as promising light sources for novel miniaturized gas-sensing systems.

1 Introduction

Mid-infrared (IR) gas-sensing technology has a large market worldwide, which can apply to fields such as process control, biomedical, environmental, and safety monitoring [1, 2]. The systems based on such technology have strong demand for continuous-wave (CW) mid-IR light source that is miniaturized, low cost, low power consumption, and with sufficient output power in the milliwatts (mW) range. In addition, low cost and low power consumption requirements also make room-temperature operation a necessity in order to avoid bulky and expensive cooling equipment, and additional driving powers. Generally, mid-infrared light sources can be grouped into thermal and photonic technologies [3]. Thermal emitters generate photons by heat radiation. The output characteristics are majorly determined by the heating temperature as described by Planck's Law. Although low cost and high output power makes broadband hot filament thermal light sources, the primary choice in the market, their low efficiency, high power consumption, poor frequency modulation ability, and low device stability severely limit their applications.

Instead, solid-state photonic emitters including light-emitting diodes (LEDs) and laser diodes generate photons by the radiative recombination of electrons and holes. Their bandwidth can vary from fairly wide (LEDs) to very narrow (laser diodes). This type of light sources can offer higher efficiency, smaller size, lower power consumption, and faster tuning operation compared to thermal emitters. Mid-IR lasers, which are currently dominated by quantum cascade lasers, can provide high output power and miniature properties [4]. But unfortunately, these devices are difficult and costly to fabricate. By contrast, mid-IR LEDs are less expansive and easier to fabricate compared to lasers. However, the output powers that III–V-based mid-IR LEDs provide are below mW range [3, 5], which limits their applications. Therefore, to improve the efficiency of mid-IR LEDs with enhanced output power is of great research interests.

✉ Binbin Weng
binbinweng@ou.edu

Zhisheng Shi
shi@ou.edu

[1] The School of Electrical and Computer Engineering, University of Oklahoma, Norman, OK 73019, USA

[2] Nanolight Inc., Norman, OK 73069, USA

Published online: 26 December 2016

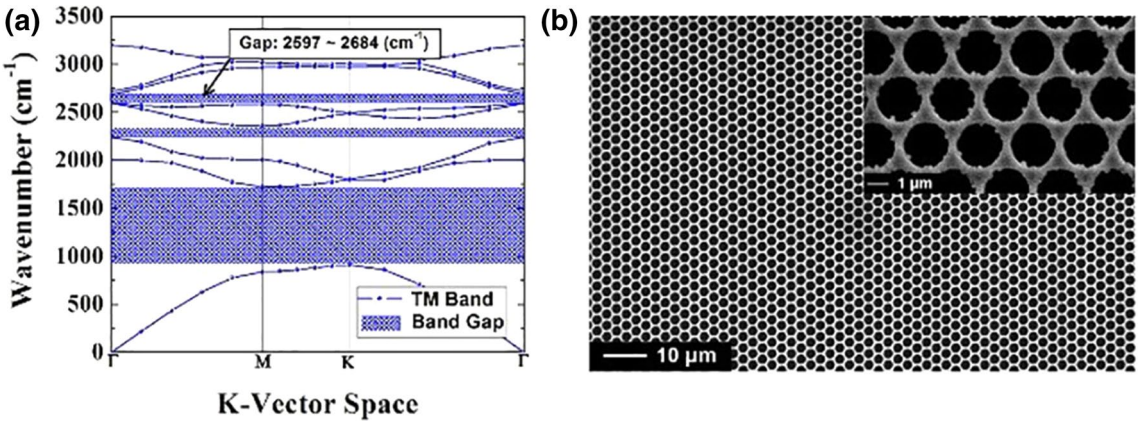

Fig. 1 **a** TM modes dispersion diagram of the 2D hexagonal photonic crystal array and **b** *top-view* SEM image of PbSe/PbSrSe MQWs structure grown on patterned Si (111). *Note:* the *inset* shows the higher magnification SEM image of (**b**)

As one of the major mid-IR semiconductor materials, lead-salt semiconductors have been intensively investigated for developing mid-IR light sources at room-temperature or near-room-temperature range, due to their unique properties such as direct narrow band gaps with strong mid-IR light absorption coefficients and low Auger recombination rates [6–8]. However, for planar structure, the total reflective resonant cavity created by their large refractive indices [9] largely limits the light extraction efficiency. Therefore, a surface-structuring method was successfully implemented and increased the emission power up to 2 mW [6, 7, 10].

Compared to the traditional surface-structuring method, a new surface engineering technique called "the photonic crystal" has been rapidly developed in the past decade, mainly due to its ability to effectively manipulate photons nonlinearly. In our group, we have demonstrated research works incorporating photonic crystal structure with lead-salt material for mid-IR light emitters development, and significant emission improvement and even laser behavior under pulse mode operation have been observed [11, 12]. However, the pumping source used was a high-power pulsed Nd:YAG laser which is bulky, expensive, and with very high power consumption. In addition, no CW photonic crystal emission was clearly observed. Therefore, in this paper, we apply a new design strategy (note: the details will be described in the following section) to investigate and successfully develop a diode-pumped mid-IR light source operating under the CW mode at room temperature.

2 Design and experiments

In order to design a photonic crystal array capable of modulating mid-IR light around 3–4 μm, we used a commercial software package, OPTIFDTD, to analyze the in-plane photonic energy band structure by the plane-wave expansion method. The design parameters included the refractive index n of the epitaxial material, the inter-hole spacing a, and the radius of the air holes R. A two-dimensional hexagonal holes array ($a = 2.5$ μm and $R = 1.10$ μm) was constructed to form a photonic band gap from 2684 (3.72 μm) to 2597 cm^{-1} (3.85 μm) in order to match up with the peak of the optical gain of the PbSe/PbSrSe (9.5/25 nm) quantum wells at room temperature. The band diagram is demonstrated in Fig. 1a.

In our previous reports [11, 12], microcavities were fabricated by intentionally removing a hole from the photonic crystal array to create an optical state within the photonic band gap. At this defect mode, a laser behavior under pulse excitation was observed. However, the pumping power to generate such defect mode emission was very high. The threshold pumping density of the laser was 24 kW/cm^2 [12], which is much higher than most of the single CW semiconductor laser can provide. Therefore, to develop a low-cost diode-pumped CW photonic crystal mid-IR light source, a new approach utilizing the photonic crystal band-edge resonant mode was adopted in this work to enhance the light emission. Such emission does not require creating microcavity defect in the photonic crystal structure. This approach was built upon the enhanced local density of electromagnetic states associated with the critical points of the photonic band dispersion diagram. It was found that near the band-edge critical points, the slope of the band is very small, and the optical group velocity would approach to zero [13]. This property makes band-edge mode a preferable optical resonance mode in achieving enhanced nonlinear effect or low threshold light emission. Additionally, it is known that the photonic crystal defect mode mechanism only requires a small period of a holes array surrounding the microcavity (e.g., 15–20 cycles) to achieve good optical confinement. In our previous publications, a period of 30 cycles was fabricated. However, because the

photonic band-edge mode requires optical coherence across the whole photonic crystal array, limited by the small area of the photonic crystal pattern in our previous works, the band-edge mode assisted CW emission was too weak to be observed. So in this work, the period of the pattern increases to 1000 cycles in order to strengthen the band-edge mode coupling intensity.

In the experiment, 9 pairs of the PbSe/$Pb_{0.96}Sr_{0.04}Se$ quantum wells were grown on the Si substrate by molecular beam epitaxy method. Prior to the growth, a photonic crystal holes array was patterned by electron beam lithography and etched down by 3 μm using a deep reactive ion etching system on Si(111) substrate. The gases SF_6 (~300 sccm) and C_4F_8 (~150 sccm) were introduced during the etching process. JEOL JSM-6060 scanning electron microscopy (SEM) was used to characterize the morphology. In this work, the CW spectral emission performance of the as-grown PbSe/$Pb_{0.96}Sr_{0.04}Se$ quantum wells film was characterized by Bruker IFS-66v Fourier transform infrared spectroscopy system (FTIR). A high-power CW semiconductor laser with the emission peak position at 913 nm was used as the optical pump source. A standard blackbody source at 800 K was applied for the power calibration. A liquid-nitrogen-cooled InSb detector with cutoff response at around 5.2 μm was used for collecting signals. The CW pumping power ranged from 0.5 to 5.5 W, and the spot area on the sample was about 0.07 cm^2.

3 Results and discussion

Figure 1b shows a top-view SEM image of a photonic crystal patterned area with the microcavity on Si substrate after MBE growth. As can be seen, the film grown on the photonic crystal top structure is very smooth. Our previous research found out that the material quality is actually improved greatly in this scenario [14, 15]. But compared with the theoretical design and the real processed pattern, we found the diameter of the holes was actually over-etched by 80 nm which caused a blueshift of the photonic crystal modulation modes from ~3.8 to 3.5 μm. As a result, the band-edge modes cannot perfectly match up with the peak of the gain of the quantum wells at room temperature which can significantly limit the device performance in this work.

Figure 2 presents the calibrated emission results from a planar area and a photonic crystal patterned area of this film. It needs to be mentioned that even though the background signal disturbance has been deleted from the measurement, we can still observe the thermal radiation as shown in both Fig. 2a, b. This phenomenon is due to the heating effect caused by the high-power pumping laser. The more energy with which the laser power hits on the sample,

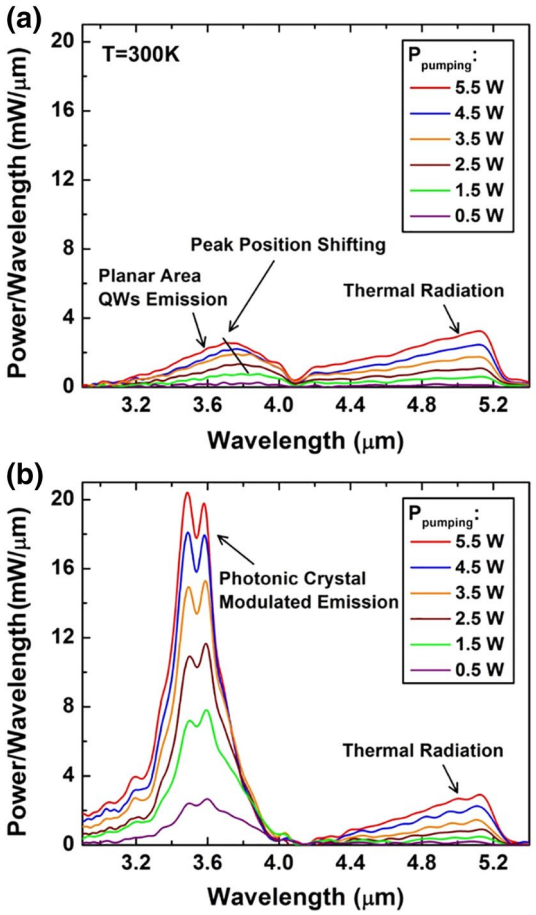

Fig. 2 Optically pumped spectra power emission from **a** planar area, and **b** photonic crystal holes array patterned area of PbSe/$Pb_{0.96}Sr_{0.04}Se$ QWs epitaxy film on Si(111) substrate

the higher thermal radiation it emits. As shown in Fig. 2a, the quantum wells demonstrate very weak spontaneous emissions whose intensities are as low as the thermal radiation levels. The peak position has a blue shifting effect due to the same heating reason as the observed thermal radiation, since PbSe material has a large positive temperature-dependent energy band gap coefficient.

On the other hand, when the photonic crystal holes array patterned area is optically pumped instead of the planar area, the sample presents much stronger emissions as shown in Fig. 2b, as compared to those of planar area. There are two emission peaks exhibited at 3.58 and 3.49 μm, respectively, which do not show the obvious peak position moving phenomenon like Fig. 2a under different pumping powers. As we stated in the theoretical simulation section, these two emission peaks are actually defined by the upper and lower band-edge optical modes in the designed photonic crystal band gap.

In addition, it is noticed that there is a photonic band gap in the 2200–2300 cm^{-1} (4.3–4.5 μm) from the theoretical

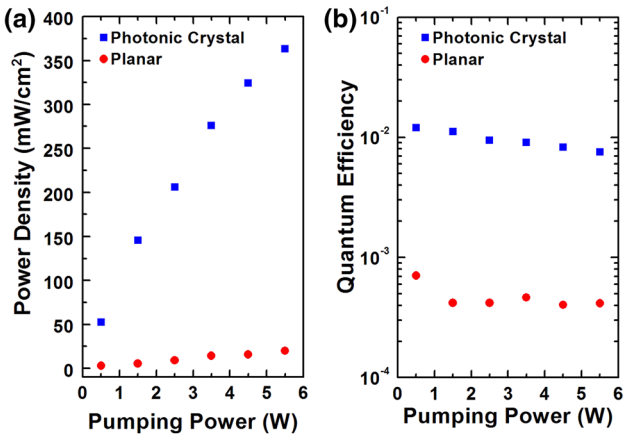

Fig. 3 **a** Emission power densities and **b** quantum efficiencies of the PbSe/$Pb_{0.96}Sr_{0.04}Se$ quantum wells from planar area and photonic crystal patterned area of the film

simulation as shown in Fig. 1a. Although this gap locates in the thermal emission spectrum, no band-edge mode modulated emission enhancement can be observed. The possible reason is that the thermal emission was mainly generated from the Si substrate rather than the epitaxial active layer. Specifically, as shown in Fig. 1b, quantum well material was only deposited on top of the membrane, while the Si substrate was still exposed to the pumping laser in the area where the holes are. Therefore, only partial laser pumping energy can couple with the active lead-salt material. By calculating the ratio between the areas taken up by the holes to the entire area, only 30% laser energy illuminated onto the epitaxial film. The remaining 70% of the energy was directly sent to the bottom thick Si substrate and transform into heat. And because the photonic band gaps were only designed for lead-salt layer based on its high refractive indices, the thermal emission from Si substrate will not be modulated by the photonic crystal structure.

Figure 3 shows the emission power densities and the quantum efficiencies from the photonic crystal patterned area and the planar area of the sample. In the photonic crystal structure, the area taken by empty holes had no light emission contribution. Therefore, as described above, the effective emission area of the photonic crystal structure is much smaller than the emission area of the planar sample without the photonic crystal pattern. Taking this factor into consideration, it is more reasonable to compare the emission powers per area (power densities) rather than the absolute power values. Thus, the emission power densities are presented in Fig. 3a. As clearly shown in the figure, the power density emitted from the photonic crystal patterned area not only is much greater but also increases faster than the one from the planar area of the sample. Besides, it is worth noting that although the strongest power density obtained from the photonic crystal area is ~363 mW/cm^2 (the corresponding power value measured is about 7.68 mW) under the 5.5-W CW laser pumping condition, the power density increasing slope actually decreases with the pumping power. It is suggested that the aggravated heating effect under higher pumping power, which is demonstrated in Fig. 2, degrades the light-emitting performance in this phenomenon.

For evaluating the quantum efficiencies (η_{quantum}), these values are retrieved from the overall efficiency (η_{overall}) equation as expressed:

$$\eta_{\text{overall}} = P_{\text{emit}}/P_{\text{pump}} = \eta_{\text{quantum}} \cdot \eta_{\text{pumping}} \cdot \eta_{\text{coupling}}$$

in which P_{emit} and P_{pump} are the emitting and pumping powers, and η_{pumping} and η_{coupling} stand for pumping and coupling efficiencies, respectively. η_{pumping} is the ratio of the pumping laser's photon energy and the energy band gap of a material. Here we only assume that one pumping photon generates one electron–hole pair. The coupling efficiency considers the reflective losses (~38%) at the boundary of Air-PbSe, and the effective pumping area ratio (~30%) in which the area taken up by holes will not be counted as mentioned previously. It needs to be mentioned that the transmission loss on the light traveling path in the testing system is neglected, which will make the estimated value a bit lower than the real one. As shown in Fig. 3b, the quantum efficiencies of quantum wells at the planar area of the sample range from 0.04 to 0.07% under different pumping powers. By contrast, the quantum efficiencies of quantum wells that photonic crystal array modulated are greatly boosted to the levels varying from 0.75 to 1.20%. Compared to the quantum efficiencies from the planar area, the highest enhancement is achieved over 26.5 times under the 1.5 W laser pumping condition. As shown in Fig. 3a, quantum efficiency also decreases with the pumping power, which suggests that the performance can be improved with an efficient heat sink attached. Secondly, as we mentioned before, due to the dimension control variation of the DRIE process, the photonic crystal modes cannot match up with the gain peak of the quantum wells at room temperature. In addition, as indicated in the inset of Fig. 1b, the zigzag microcrystals extended from the edges of the holes, caused by the imperfections of the DRIE process on Si wafer, play major leak channels in the photonic crystal modulated light resonating mechanism. In this case, much higher quantum efficiency or even a CW laser performance can be anticipated if those problems are solved.

4 Conclusion

In conclusion, we present a photonic crystal enhanced lead-salt light emitter operated under CW mode at room

temperature. Under optical pumping by a CW 913-nm semiconductor laser, the photonic crystal assisted device exhibits strongly enhanced light emission performance compared to the regular one without photonic crystal structure integration. This technology offers a mid-IR light emitter with high emission powers at room temperature which is critical for optoelectronic applications, specifically for gas-sensing devices.

Acknowledgements We acknowledge financial support from the DoD ARO Grant No. W911NF-07-1-0587 for this work.

References

1. P. Werle, F. Slemr, K. Maurer, R. Kormann, R. Mucke, B. Janker, Near- and mid-infrared laser-optical sensors for gas analysis. Opt. Lasers Eng. **37**(2–3), 101–114 (2002)
2. J. Hodgkinson, R.P. Tatam, Optical gas sensing: a review. Meas. Sci. Technol. **24**, 59 (2013)
3. G.Y. Sotnikova, G.A. Gavrilov, S.E. Aleksandrov, A.A. Kapralov, S.A. Karandashev, B.A. Matveev, M.A. Remennyy, Low voltage CO_2-gas sensor based on III–V mid-IR immerson lens diode optopairs: where we are and how far we can go? IEEE Sens. J. **10**, 225–234 (2010)
4. A. Kosterev, G. Wysocki, Y. Bakhirkin, S. So, R. Lewicki, M. Fraser, F. Tittel, R.F. Curl, Application of quantum cascade lasers to trace gas analysis. Appl. Phys. B: Lasers Opt. **90**, 165–176 (2008)
5. B.A. Matveev, G.A. Gavrilov, V.V. Evstropov, N.V. Zotova, S.A. Karandashov, G.Yu. Sotnikova, N.M. Stus, G.N. Talalakin, J. Malinen, Mid-infrared (3–5 μm) LEDs as sources for gas and liquid sensors. Sens. Actuators B Chem. **39**, 339–343 (1997)
6. F. Weik, J.W. Tomm, R. Glatthaar, U. Vetter, D. Szewczy, J. Nurnus, A. Lambrecht, L. Mechold, B. Spellenberg, M. Bassler, M. Behringer, J. Luft, Midinfrared luminescence imaging and its application to the optimization of light-emitting diodes. Appl. Phys. Lett. **86**, 041106 (2005)
7. J. Nurnus, U. Vetter, J. Koenig, R. Glatthaar, A. Lambrecht, F. Weik, J.W. Tomm, *"Optically Pumped Mid Infrard Emitters Built Using Surface Structured PbSe epitaxial Layers," in SPIE-Photonic Materials* (Devices and Applications, Bellingham, WA, 2005)
8. M. Böberl, W. Heiss, T. Schwarzl, K. Wiesauer, G. Springholz, Midinfrared continuous-wave photoluminescence of lead–salt structures up to temperatures of 190°C. Appl. Phys. Lett. **82**, 4065 (2003)
9. J.N. Zemel, J.D. Jensen, R.B. Schoolar, Electrical and optical properties of epitaxial films of PbS, PbSe, PbTe, and SnTe. Phys. Rev. **140**, A330 (1965)
10. F. Weik, G. Steinmeyer, J.W. Tomm, R. Glatthaar, U. Vetter, J. Nurnus, A. Lambrecht, A room-temperature continuous-wave operating midinfrared light emitting device. J. Appl. Phys. **99**, 114506 (2006)
11. B. Weng, J. Ma, L. Wei, J. Xu, G. Bi, Z. Shi, Mid-infrared surface-emitting photonic crystal microcavity light emitter on silicon. Appl. Phys. Lett. **97**, 231103 (2010)
12. B. Weng, J. Ma, L. Wei, L. Li, J. Qiu, J. Xu, Z. Shi, Room temperature mid-infrared photonic crystal surface emitting laser on Si. Appl. Phys. Lett. **99**, 221110 (2011)
13. F. Bordas, M.J. Steel, C. Seassal, A. Rahmani, Confinement of band-edge modes in a photonic crystal slab. Opt. Exp. **15**, 10890 (2007)
14. F. Zhao, J. Ma, B. Weng, D. Li, G. Bi, A. Chen, J. Xu, Z. Shi, MBE growth of PbSe thin film with a 9×10^5 cm^{-2} etch-pits density on patterned (111)-oriented Si substrate. J. Cryst. Growth **312**(19), 2695 (2010)
15. B. Weng, F. Zhao, J. Ma, G. Yu, J. Xu, Z. Shi, Elimination of threading dislocations in as-grown PbSe film on patterned Si (111) substrate using molecular beam epitaxy. Appl. Phys. Lett. **96**(25), 251911 (2010)